Research Article

Atmospheric aerosol properties at a semi-rural location in southern India: particle size distributions and implications for cloud droplet formation

S. Shika[1] · H. Gadhavi[2,3] · M. N. S. Suman[2,4] · R. Ravikrishna[5] · Sachin S. Gunthe[6]

Received: 16 November 2019 / Accepted: 22 April 2020 / Published online: 3 May 2020

Abstract
Particle number size distributions in the diameter range of 5 nm–34 µm were measured in tropical southern India during the transition season from May (pre-monsoon) to June–July (monsoon). Averaged over the entire measurement period, the particle number size distributions were bimodal with a total particle number concentration of $N_{Tot} = (4.5 \pm 2.7) \times 10^3$ cm^{-3} (arithmetic mean ± standard deviation). The ratio of Aitken to accumulation mode particle number concentrations (N_{Ait}/N_{Acc}) ranged from 1.06 to 2.07, increasing from May to June–July due to a pronounced decrease in the accumulation mode particles with the onset of the monsoon. Cloud condensation nuclei concentrations at 0.4% supersaturation ($CCN_{0.4}$) were calculated under the assumption of an average continental hygroscopicity parameter of $\kappa = 0.3$. The calculated $CCN_{0.4}$ concentrations are mostly sensitive to variations in N_{Acc} and vary accordingly between the May and June–July. Using a cloud parcel model, we investigated the formation of cloud droplets using the measured average particle number size distributions, updraft velocities up to 20 m s^{-1}, and initial aerosol particle number concentrations up to 25,000 cm^{-3}. We found different regimes of CCN activation and cloud formation for the month of May (shifting from aerosol-limited regime to transitional regime) and for June–July (transitional regime), which was primarily due to the variability of particle number concentrations in the accumulation mode.

Keywords Size distribution · Cloud condensation nuclei · Cloud parcel modelling

1 Introduction

Atmospheric aerosol particles can significantly affect the climate system by directly interacting with the incoming solar radiation and by serving as cloud condensation nuclei (CCN) for the formation of cloud droplets. Thus, aerosol particles play an important role in the Earth's radiation budget and can potentially influence cloud microphysical properties, cloud lifetime, and precipitation, thereby affecting the hydrological cycle [1, 4, 49]. The properties of aerosols are highly variable in space and time, and hence their effects on climate, visibility, and human health are different from place to place and season to season [2, 3]. The largest variations are observed in the particle number concentration, which varies from a less than one particle per cm^3 in the remote Arctic to a few hundred particles

Electronic supplementary material The online version of this article (https://doi.org/10.1007/s42452-020-2804-2) contains supplementary material, which is available to authorized users.

✉ S. Shika, shikasuren@gmail.com; ✉ Sachin S. Gunthe, s.gunthe@iitm.ac.in | [1]Department of Civil Engineering, Vimal Jyothi Engineering College, Kannur, Kerala, India. [2]National Atmospheric Research Laboratory, Gadanki, Tirupati, India. [3]Present Address: Physical Research Laboratory, Navrangpura, Ahmedabad, India. [4]Present Address: CNRM/GMME, CNRS, Meteo-France, Toulouse, France. [5]Department of Chemical Engineering, Indian Institute of Technology Madras, Chennai, India. [6]EWRE Division, Department of Civil Engineering, Indian Institute of Technology Madras, Chennai, India.

per cm^3 in the pristine Amazonian region to more than ten thousand particles per cm^3 in highly polluted megacities [2, 16–18, 22, 23, 29, 35, 37, 48, 53, 25, 26]. Some of the earlier studies, as mentioned below, conducted in different parts of the world, reveal the importance of measurements of number size distributions of particles with diameter smaller than 250 nm, which is often the minimum diameter of particles that can be measured with commercially available optical particle counters (OPCs). The OPC measurements for particle size greater than 250 nm may not be helpful in understanding the effect of particle number size distribution on regional climate for a given environment, as more than 90% of the particles have diameters less than 250 nm and most importantly such measurements cannot capture the new particle formation events, which constitute a large fraction of atmospheric aerosols [28, 31, 32, 57]. For example, Fig. S1 shows representative particle number size distributions taken from the available literature for various environments. Some of the recent studies carried out in India report on the influence of aerosols on cloud properties during the Indian summer monsoon season. These studies indicate the importance of aerosols involving complex interactions between direct radiative forcing, large-scale dynamics, and cloud microphysics. The enhanced aerosol concentration can modify the micro- and macro-properties of clouds and can result in an aerosol-induced cooling or warming of the atmosphere [17, 20, 30, 40, 50, 54]. Thus, data on particle number size distribution can provide important additional information for investigating the impact of aerosol particles on climate. The corresponding fit parameters for the particle number size distributions shown in Fig. S1 are given in Table 1, including the present study carried out at Gadanki [5, 16, 17, 30, 34, 54, 21].

The activation of aerosol particles as CCN is an important microphysical process for the formation of cloud and precipitation [49]. In recent times, the increasing aerosol concentration over the Indian region has been shown to affect the Indian summer monsoon in direct and indirect ways. The continental aerosols over the Indian region can alter the cloud properties in diametrically opposite ways during contrasting monsoon years [40, 20, 30, 43, 50]. The knowledge of particle size along with their hygroscopicity and the updraft velocity at the cloud base are important in understanding the process leading to CCN activation, and cloud and precipitation formation [1, 8, 45]. Petters and Kreidenweis [41] introduced the hygroscopicity parameter, κ, to represent the insoluble and soluble fraction of particles, which can be determined experimentally. For ambient aerosols, the value of κ ranges between 0.1 and 0.9. The corresponding CCN critical diameter for commonly observed supersaturations in clouds (~ 0.4%) ranges between 70 and 200 nm [1, 41]. The variability in particle size has the strongest impact on the ability of aerosol particles to act as CCN [11, 16, 33, 48, 10].

Studies over the Indian region suffer from a lack of aerosol size distribution data for validation. The measurements of particle number size distributions including the size range below 250 nm over the Indian region are sparse and often restricted to a single geographical location and part of a season [22, 38]. Some of the early studies on aerosol size distribution in the range below 250 nm diameter over Indian regions are by Jayaraman et al. [23] and Ganguly et al. [15], etc.; however, they are restricted to short campaign periods and a few locations. In an effort to characterize the particle number size distribution in southern tropical India, we conducted a field campaigns at Gadanki (13.46° N, 79.17° E, 336 amsl), a semi-rural site in southeastern India during May–July 2012.

Table 1 Fitted parameters of the number size distribution from various contrasting environments across the globe, displaying both monomodal and bimodal distributions

Sampling location	Lat	Long	N_1	σ_1	D_{g1}	N_2	σ_2	D_{g2}
Remote marine								
(a) Northern hemisphere	75 N	90 E	160	1.5	45	60	1.6	170
(b) Tropics	0 N	15 E	280	1.6	46	240	1.5	160
(c) Southern hemisphere	60 S	75 W	310	1.4	35	70	1.6	150
China			1987	1.752	87.3	–	–	–
Coastal Mediterranean			483	1.781	82.94	–	–	–
Antarctica	74.5 N	163.45 E	318	1.35	21.7	187	2.02	56.2
Beijing	39.515 N	116.305 E	15,600	2.8	75	–	–	–
Amazon	2.505 S	61.209 W	97	1.49	57.3	95	1.43	168
Nepal	27.601 N	85.538 E	6459	2.303	78.88	–	–	–
Gadanki[a]	13.459 N	79.168 E	1524	2.1	26.45	2850	2	68.5

[a]Present study

2 Methodology

2.1 Measurement site and meteorology

Measurements were carried out at Gadanki for a period of 90 days from 2 May to 31 July 2012 at the National Atmospheric Research Laboratory (NARL) close to Gadanki, a small village in the Chittoor District in Andhra Pradesh, which is a semi-rural continental site with a total population of 2586 (Fig. 1). A national highway (NH 18), which is the only potential source for local anthropogenic particle emissions, passes near to the observation site with a frequency of around more than a hundred heavy vehicles per day. As reported by previous studies [14, 25, 26], no direct and immediate impact of the vehicular emissions on the measurements was observed, which is probably due to the aerial distance of more than 0.5 km and altitude difference of about 50 m between the road and the actual sampling location. The instrument was installed in an open area amidst the other main facilities without obstructing the sampling at the site. The measurement location is surrounded by mountainous terrain to the north, south, and east, thus restricting any possibility of direct transport of pollutants to the observation site owing to this unique topographical feature.

The Indian tropical region, including this site, is affected by both the southwest (SW) and northeast (NE) monsoons, which is mainly caused by the north–south shift of the Intertropical Convergence Zone (ITCZ), also known as the monsoon trough. The seasonal variation was analysed by categorizing the measurement period as pre-monsoon (May) and monsoon season (June–July).

2.2 Instrumentation

Ambient aerosol particles of diameter ranging from ~ 5 nm to 34 µm were measured using a Wide-Range Aerosol Spectrometer (WRAS), GRIMM WRAS 665, with a time resolution of 5 min during the sampling period from 2 May to 31 July 2012. The WRAS comprises two units, a scanning mobility particle sizer (SMPS) and an optical particle counter (OPC). Frequently used notations and abbreviations are listed in Table S1. The entire set-up is housed in a 60 × 60 × 120 cm stainless steel housing protecting the unit from weather conditions. The WRAS inlet was situated at a height of 3 m (approx.) from the ground. The relative humidity of the aerosol particles before measurements was maintained at ~ 20% using a Nafion membrane embedded in the instrument inlet. An automatic weather

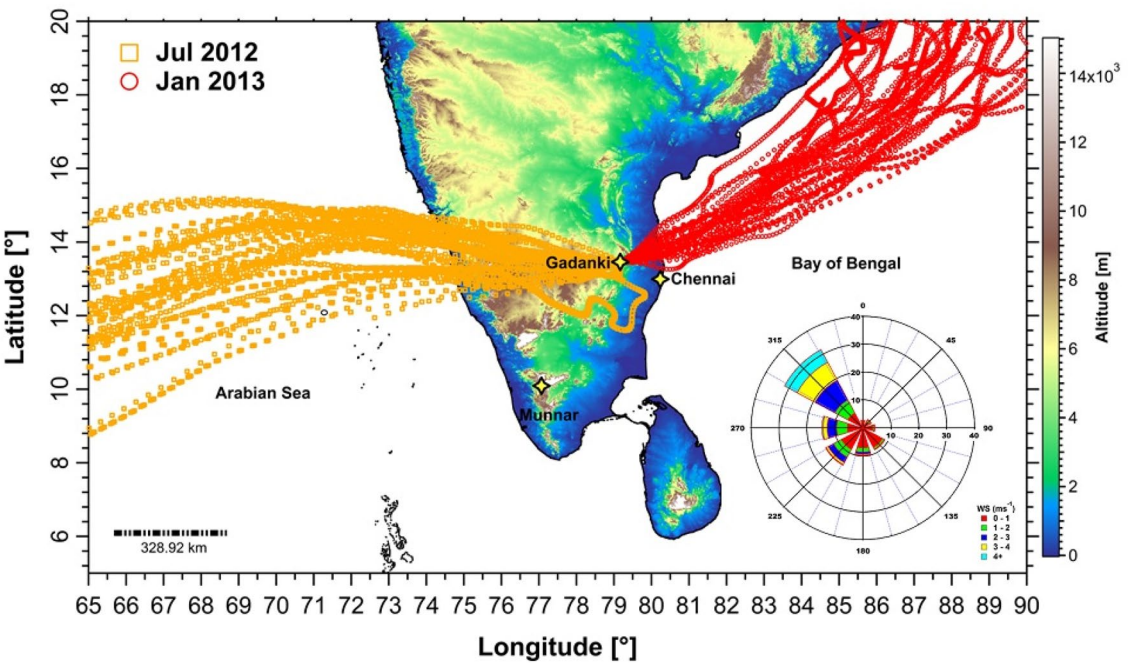

Fig. 1 Map of the southern tropical Indian region showing the area around the measurement location, Gadanki. Exemplary back trajectories obtained by the NOAA Hysplit model for Gadanki are shown for the months of July 2012 and January 2013. Due to the systematic and cyclic monsoon circulation, a unique feature of opposite direction in the prevailing wind is observed during the respective months. Colour coding of the map indicates the topography. The prevailing wind directions during the measurement period are shown in the inset

station (AWS) installed at NARL was used to acquire the meteorological data (temperature, relative humidity, wind speed, wind direction, and rainfall).

2.3 Data analysis

2.3.1 Aerosol number size distribution

The analysis of the particle number size distribution was carried out based on a lognormal distribution:

$$n_N(\log D_p) = \sum_{i=1}^{n} \frac{N_i}{\log\sigma_i\sqrt{2\pi}} \exp\left[\frac{-(\log D_p - \log D_{pi})^2}{2\log^2\sigma_i}\right] \quad (1)$$

where N_i is the total aerosol number concentration in the ith bin, D_p is the particle diameter, D_{pi} and σ_i are the geometric mean particle diameter and the geometric standard deviation, respectively, of mode i of the distribution [52]. In the present study, the particle concentrations were segregated over different size ranges: 5–25 nm (N_{Nuc}; nucleation mode particles), 25–100 nm (N_{Ait}; Aitken mode particles), 100–1000 nm (N_{Accu}; accumulation mode particles), and 5–1000 nm (N_{Tot}; total particles) [53, 57]. The number concentration of particles > 1000 nm diameter was observed to be less than 10% during the entire measurement period. Hence, the size range between 1 and 34 µm was not taken into account in this paper for any discussion of the number concentrations. Deriving the total mass concentration, however, the full size range (5 nm to 34 µm) was taken into account.

2.4 Air mass back trajectories

Back trajectory analysis was carried out to broadly categorize the origin of air masses reaching the observation site. The 48-h backward trajectories initiated at 50 m above ground level for each day during the measurement campaign were calculated using the National Oceanic and Atmospheric Administration (NOAA), Air Resource Laboratory HYSPLIT 4 model (Hybrid Single Particle Lagrangian Integrated Trajectory; [58]). Two distinct air mass types were observed reaching the observation site, of which one originated from the Arabian Sea (AS), whereas the other one originated over the Bay of Bengal (BoB), with a much shorter distance travelling over the continent. For brevity, these air mass types are referred to as AS air mass and BoB air mass throughout the manuscript. However, the two focus periods discussed here are not of equal duration. From 7 May to 14 May, BoB air masses prevailed, whereas from 15 May to 31 July AS air masses were observed.

2.5 Estimation of $CCN_{0.4}$ concentration

The hygroscopicity parameter, κ, a unitless quantity [41], can be used to describe the ability of an atmospheric particle to take up water depending on its chemical composition. The parameter κ is zero for insoluble material and around one for highly hygroscopic salts such as sodium chloride. During our measurement campaign, we did not have the possibility to measure the chemical composition of the aerosol particles or conduct other supplementary measurements to derive the values of κ. While the continental average value of $\kappa = 0.3$ was assumed [1], considering the nature of the site and changes in prevailing wind patterns we do expect some variation in the κ values during May and June–July. To understand the effect of variation in κ on the cloud droplet formation, the cloud parcel model simulation was performed for κ values varying from 0.001 to 0.7 while maintaining constant value for updraft velocity and initial aerosol number concentration for the contrasting environmental conditions. Through the simulations, it was observed that κ had a very marginal influence (< 15% for lower supersaturation of < 0.1%) on the cloud droplet concentration. Thus, size has more influence in deciding the number of cloud droplet activation over chemistry as has already been shown by previous researchers [11, 16, 48]. However, such a variation (for example 0.25–0.5) may not have a significant impact on the cloud droplet formation (less than 15%), compared to differences in number size distributions [11, 42, 45]. We calculated the CCN concentration for a supersaturation of 0.4% based on the measured particle number size distribution using the Köhler model equation as given in Eq. 2 [41, 47]. The detailed methodology is discussed elsewhere [16, 48].

$$s = \frac{D_{wet}^3 - D^3}{D_{wet}^3 - D^3(1-\kappa)} \exp\left(\frac{4\sigma_{sol}M_w}{RT\rho_w D_{wet}}\right) \quad (2)$$

The activation diameter, D, was determined by inserting the hygroscopicity parameter, $\kappa = 0.3$, and varying both D and the droplet diameter D_{wet} until the saturation ratio (s) = 1.004 and at the same time the maximum of the Köhler curve was obtained (Eq. 2). The temperature (T) and gas constant (R) were taken as 298.15 K and 8.135 J K^{-1} mol^{-1}. The droplet surface tension was approximated with that of pure water (σ_{sol} = 0.072 J m^{-2}). The density (ρ_w) and molar mass (M_w) of water were set as 997.1 kg m^{-3} and 0.018015 kg mol^{-1}. The activation diameter is thus estimated to be 66 nm for the above values, i.e. all the particles with diameter larger than 66 nm are expected to activate into cloud droplets.

2.6 Cloud parcel model simulations

The role of atmospheric aerosols is very crucial in the formation of cloud droplets by serving as CCN. The cloud parcel model used in this study was developed by Simmel et al. [55]; it comprises the Kelvin effect and Raoult's law and contains a detailed cloud microphysics spectral description [56]. The model calculates the growth of a droplet and assumes it to be a cloud droplet as soon as the particle attains a size of 1 µm. The particle growth rates were calculated based on the following equation [45, 56]:

$$\frac{dm}{dt} = \frac{4\pi r\left(s_{\infty} - s_{eq}\right)}{\left(\frac{L_v}{R_v T} - 1\right)\frac{L_v}{K^* T} + \frac{R_v T}{e_{s,w}(T) D^*}} \quad (3)$$

where m is the particle mass, t the simulation time, r the particle radius, T the temperature, L_V the latent heat of condensation (2.50078 J kg^{-1}), R_V the gas constant for water vapour (461.5 J kg^{-1}K^{-1}), K^* the modified thermal conductivity of air (Wm^{-1} K^{-1}), $e_{s,w}$ the saturation water vapour pressure, D^* the modified diffusion coefficient for water vapour in air (m^{2}s^{-1}), s_∞ the saturation ratio of the surrounding air, and s_{eq} the equilibrium water vapour saturation ratio at the particle/air interface, which is equivalent to s in Eq. 2. For more details and the parameterization of $K^*$and D^*, refer to Simmel and Wurzler [56].

In the present study, the cloud parcel model simulations were performed separately for May and June–July. Further details, like the implementation and use of the hygroscopicity parameter in the original model and subsequent model validation, are described in Reutter et al. [45].

The following input parameters were used to initialize the model simulations and to calculate the initial cloud droplet concentrations (N_{CD}): (1) The initial meteorological conditions (relative humidity, pressure, temperature, etc.), (2) the updraft velocity of the air parcel, which was varied from 0.1 to 20 m s^{-1}, (3) the dry aerosol particle number size distribution in terms of geometric mean diameter (D_g), standard deviation (σ_g), and initial aerosol particle number concentration, which was varied from 5 to 25,000 cm^{-3}, and (4) the hygroscopicity parameter, with assumption of a continental average of 0.3.

Based on the ratio between updraft velocity (ω) and particle number concentration (N_{CN}), Reutter et al. [45] have defined three distinct cloud formation regimes, i.e. an aerosol-limited regime, an updraft-limited regime, and a transitional regime. These regimes were quantitatively defined and distinguished based on the relative sensitive ratio. The border between the regimes is approximately calculated based on the ω/N_{CN} ratio. In the aerosol-limited regime, the cloud droplet number concentration (N_{CD}) is proportional to N_{CN} and independent of ω. This regime is characterized by a high maximum value of water vapour supersaturation ($S_{max} \geq 0.5\%$) and a high ω/N_{CN} ratio ($\geq 10^{-3}$ m s^{-1}cm^3). The updraft-limited regime has a low ω/N_{CN} ratio ($\leq 10^{-4}$ m s^{-1}cm^3) and a low maximum value of water vapour supersaturation ($S_{max} \leq 0.2\%$). In this regime, N_{CD} is independent of N_{CN} and proportional to ω. In the transitional regime, N_{CD} depends on both N_{CN} and ω. It is characterized by the values between the aerosol-limited and the updraft-limited regime [45].

3 Results and discussion

3.1 Aerosol particle number size distribution

Figure 2 shows the overall temporal variation of the aerosol characteristics and meteorological parameters measured for the May and June–July. The average ambient temperature for May was 31.4 ± 9.2 °C, which decreased slightly to 29.5 ± 9.4 °C over June–July due to rain and persistent cloud cover. In contrast, the relative humidity (RH) exhibited a slight increase during the monsoon season (59 ± 24%) compared to May (53 ± 22%). The variation in the wind speed was not very significant between the two seasons. The total particle concentrations (N_{Tot}) averaged for the months of May, June, and July were $(5.8 \pm 2.6) \times 10^3$, $(4.3 \pm 2.7) \times 10^3$, and $(3.9 \pm 2.4) \times 10^3$ cm^{-3}, respectively. It was highest in May and gradually decreased with the onset of the monsoon from June, due to scavenging and wet deposition [25, 26]. A diurnal variation in the meteorological and aerosol parameters (N_{Tot}, D_g, σ_g, etc.) was clearly evident and was more pronounced during the month of May. The average D_g during May was 86 ± 36 nm, which decreased to 41 ± 38 and 47 ± 31 nm during the monsoon months of June and July, respectively. The average particle number concentration observed at this site was found to be in good agreement with other semi-rural and background sites in various other parts of the globe, including Denmark and the USA [2, 24, 62]. Similar to values reported by Tunved et al. [60] at a Swedish background site, the aerosol particle number concentration was observed to be in the range of 1100–5200 cm^{-3}. At other semi-rural sites, the particle number concentration had been found to be as high as 10,000 cm^{-3} [24].

Figure 3 shows the average particle number size distributions for the months of May (a), June (b), July (c), and the entire measurement period (d). The median particle number size distribution during May exhibited a monomodal distribution with a geometric mean

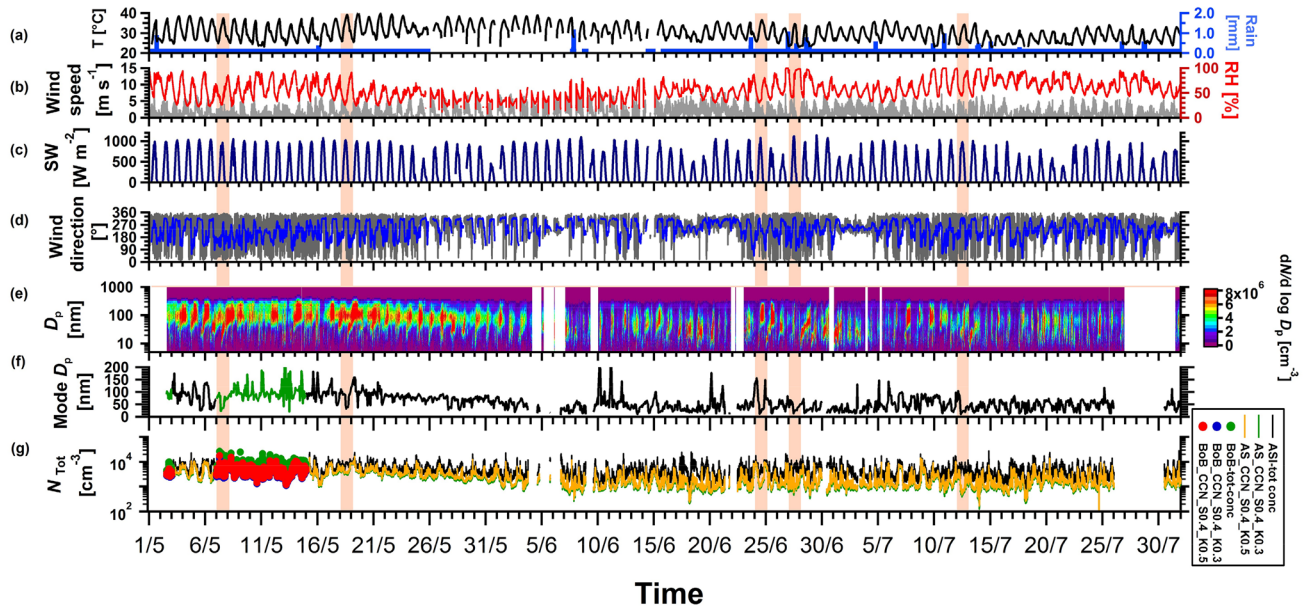

Fig. 2 Time series of the measured meteorological and aerosol parameters during 2 May–31 July 2012: **a** air temperature (T, black) and daily rainfall (Rain, blue), **b** wind speed (grey) and relative humidity (RH, red), **c** shortwave radiation (SW, blue), **d** wind direction (5 min average, grey and hourly average, blue), **e** contour plot of particle number size distributions ($dN/d\log D_p$), **f** hourly modal diameter (Mode D_p) of the two air masses (BoB air mass, green and AS air mass, black), and **g** number concentration of particles in the size range of 5–1000 nm (N_{Tot}) and of CCN. The vertical bars indicate the observed NPF event days

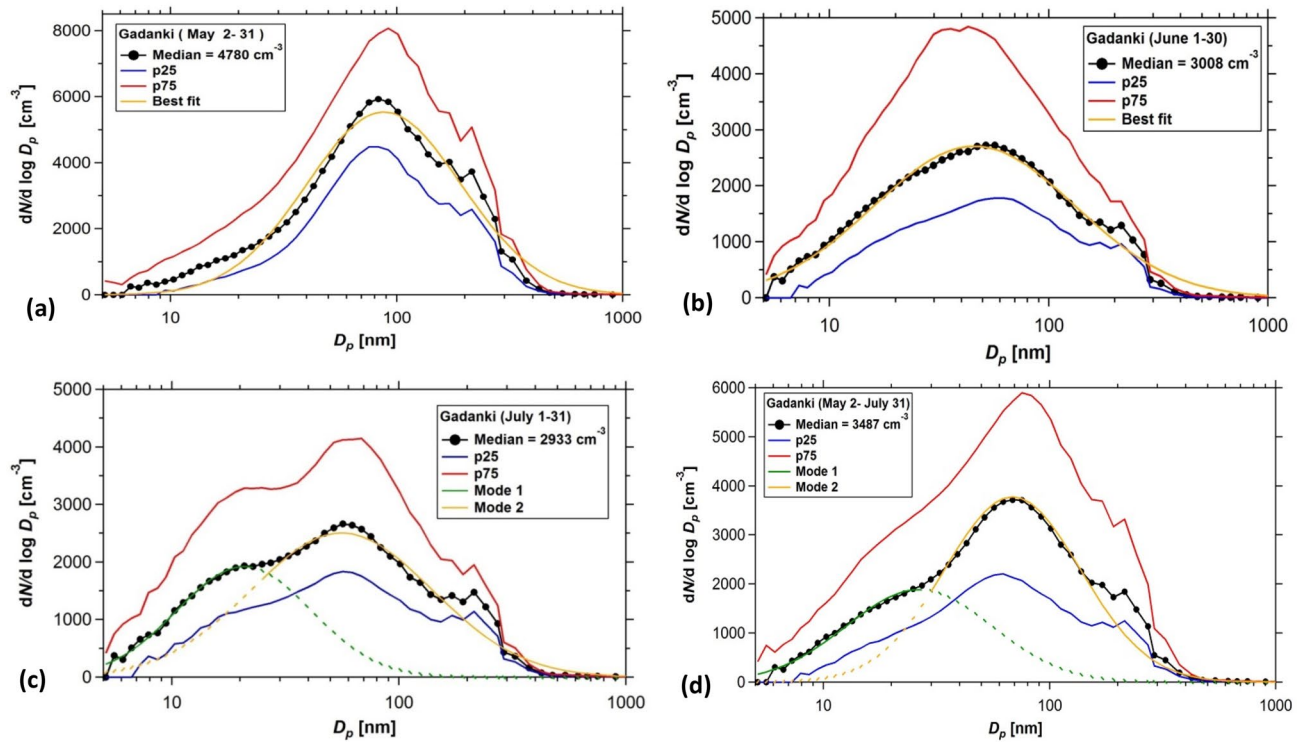

Fig. 3 Median particle size distribution for the months **a** May, **b** June, **c** July and **d** total of 3 months together with the 25th (blue) and 75th (red) percentile distribution. The presence of a yellow line only indicates a monomodal fit, and the presence of both yellow and green lines represents a bimodal fit

diameter, D_g, of 88 ± 1.4 nm and a standard deviation, σ_g, of 2.19 ± 0.03 nm, obtained by fitting Eq. 1 (WaveMetrics IGOR Pro version 6.22A). The particle number size distribution during May was narrower compared to the other two monsoon months. In June, the geometric mean diameter and standard deviation of the number size distribution were $D_g = 46 \pm 0.6$ nm and $\sigma_g = 2.88 \pm 0.04$ nm, respectively. Changes in the geometric mean diameter of the particle number size distribution for a given observation site most likely reflect the different particle emission sources and ageing histories. We observed that, while the particle number concentration was still dominated by Aitken mode particles during June, the nucleation mode exhibited an increase in particle number concentration. Interestingly, the particle number concentration during July (Fig. 3c) was bimodal in nature. The peak in the nucleation mode was observed at ~ 25 nm and the Aitken mode peaked at ~ 50 nm, with a total particle number concentration of 3300 ± 2600 cm^{-3}, which is comparable to the monsoon month of June and around 15% less than the particle concentration observed in May. The difference in the overall nature of the particle number size distribution between May and June–July could be explained based on the prevailing winds arriving at the observation site and perturbations of the air mass on the way due to activities upwind.

The averaged particle number size distribution over the entire measurement period is shown in Fig. 3d. The overall particle number size distribution was bimodal with a first peak in the nucleation mode at around 26 nm and a second peak in the Aitken mode at 69 nm. In a campaign conducted by Kopanakis et al. [30] at a rural/suburban site in the eastern Mediterranean, the distribution was observed to be similar to our study region, being monomodal in summer and bimodal in the remaining period. The arithmetic mean daytime and nighttime particle number size distributions for the month of May are shown in Fig. S2. It is evident from this figure that the shape of the particle number size distribution did not exhibit significant differences between daytime and nighttime, similar to a site in the Himalaya mountain range in Nepal [54].

Variations in the contributions of the different particle modes during May and June–July indicated a potential difference in the particle characteristics over this region during the two distinct meteorological seasons. To elucidate this further, the average relative contribution of the number concentration in the three different modes for the individual months and the entire campaign is shown in Fig. 4. It is evident that the relative contribution of nucleation mode particles was only 13% in May, whereas Aitken and accumulation mode particles constituted 45% and 42% of the total particle number concentration, respectively.

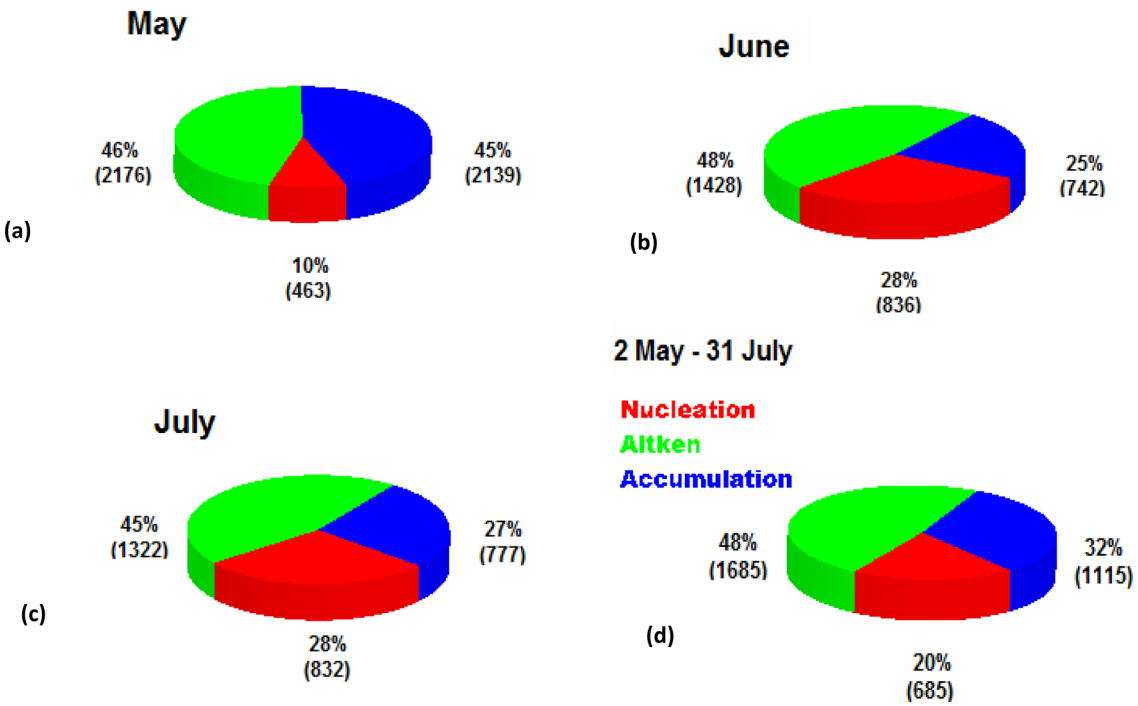

Fig. 4 Relative distribution of particle number concentrations (with the absolute number concentration in parentheses) in the nucleation, Aitken and accumulation modes for the observation period, showing higher prevalence of accumulation mode particles in May, which decreased in June and July

In June and July, the relative concentration of nucleation mode particles increased to 30% and 29%, respectively, and the accumulation mode particles for the same months decreased roughly to half of that observed in May (23% and 26%, respectively). This decrease in the accumulation mode particles for June and July is further evident from the normalized size distributions for the three individual months (Fig. S3). The number concentration of particles observed in the Aitken mode did not exhibit any significant variation during the entire measurement period. The higher ratios of Aitken to accumulation mode number concentration (N_{Ait}/N_{Accu}) are generally associated with new particle formation events and freshly emitted aerosol particles [6]. N_{Ait}/N_{Accu} was slightly greater than one (1.07) during May and increased with the arrival of the monsoon season to values of 2.04 and 1.73 for June and July, respectively. The averaged ratios of N_{Ait}/N_{Accu} at Mukteshwar and Gul Pahari were 0.58 and 0.65 [22], respectively. Biagio et al. [6] reported very high ratios of N_{Ait}/N_{Accu} in the range of 5–15 and attributed such high ratios to the fresh emissions from a strong local source. In various high-altitude regions with free tropospheric atmospheric conditions, the N_{Ait}/N_{Accu} ratio was in the range of 1–5 [39]. Although it was observed that the total number concentration during the monsoon season was lower compared to May, the ratio of N_{Ait}/N_{Accu} was observed to be on average higher by 70–90% in June–July due to a substantial increase in nucleation mode particles. An increase in the N_{Ait}/N_{Accu} ratio can result from an increase in the number concentration of smaller particles from NPF, as well as a decrease in accumulation mode particles due to scavenging and washout resulting from monsoonal rainfall [25, 26]. Thus, the increase in this ratio during June–July at this site is unlikely to come from fresh anthropogenic emissions. Further, changes in the prevailing wind pattern can alter the particle sources affecting the N_{Ait}/N_{Accu} ratio (Fig. S4).

3.2 Size distribution in different air masses

During the measurement period, the prevailing wind was mostly westerly, except for a few days during May when the air mass originated south of India, and travelled parallel to the eastern coast before reaching the site Thus, the size distribution was classified into two distinct air masses, viz. BoB air mass and AS air mass, based on the direction from where the 48-h back-trajectories came. Freutel et al. [13] classified air masses as Central Europe, Atlantic clean, and Atlantic polluted, and reported that air masses having higher velocity and less residence time over the continent were less polluted when compared to other air masses. In our study, the air masses originated over AS had relatively high wind speeds compared to the BoB air masses (Fig S4). Figure 5 shows the particle number size distribution for BoB and AS air masses. Note that the measurement and averaging period for the air masses were not equal. The BoB air mass exhibited a monomodal number size distribution with an average particle number concentration of $(5.9 \pm 2.2) \times 10^3$ cm^{-3}, while the particle concentration during the AS air mass was ~ 25% lower ($(4.6 \pm 1.5) \times 10^3$ cm^{-3}) with a bimodal distribution. The particle number size distribution during the BoB air mass was narrower compared to the AS air mass with a geometric mean diameter of ~ 80 nm in the Aitken mode. The bimodal number size distribution during the AS air mass exhibited a first peak at ~ 30 nm and a second peak at ~ 70 nm with particle concentrations of $(1.4 \pm 1.3) \times 10^3$ cm^{-3} and $(3.1 \pm 2.1) \times 10^3$ cm^{-3}, respectively, (with a total particle concentration of $(4.6 \pm 2.7) \times 10^3$ cm^{-3}). The peak in the lower diameter range during the AS air mass indicated the presence of smaller particles picked up by the air mass on their way.

Further, the frequency distribution of the geometric mean diameter, which was derived for each

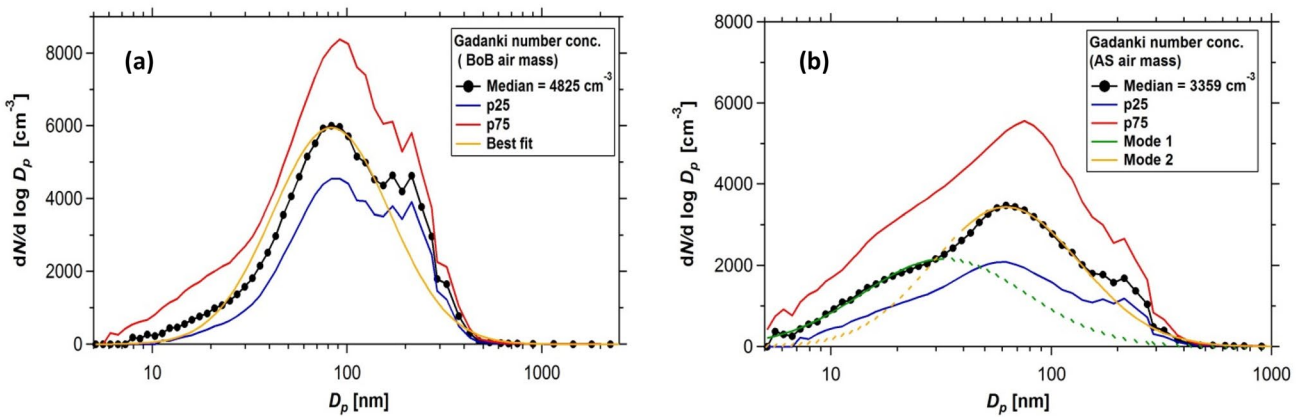

Fig. 5 Median and interquartile range of the particle number size distribution of **a** Bay of Bengal (BoB) air masses with monomodal distribution (yellow line) and **b** Arabian Sea (AS) air masses with bimodal distribution (yellow and green lines)

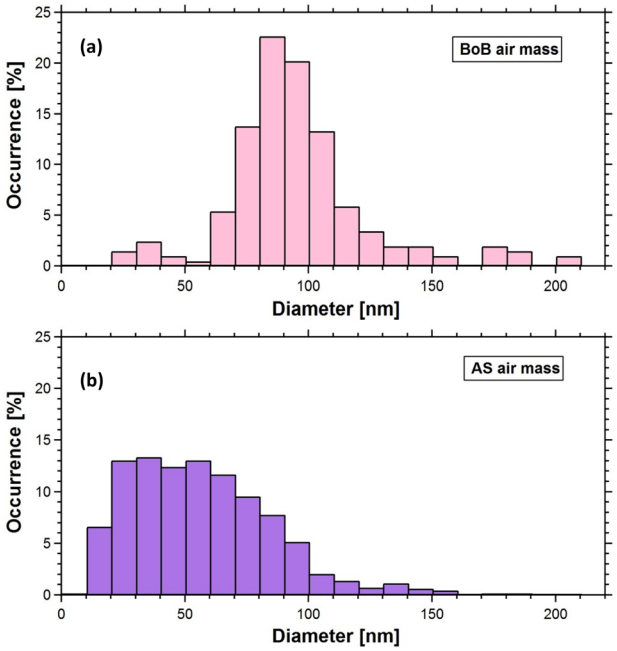

Fig. 6 Frequency distribution of the modal diameter for the two air mass types, **a** BoB air mass and **b** AS air mass

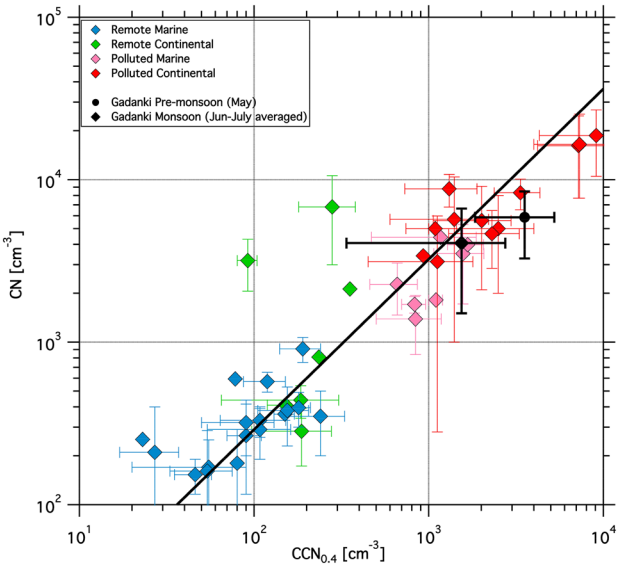

Fig. 7 Scatter plot of CN versus $CCN_{0.4}$ for pre-monsoon (black circle) and monsoon (black diamond) seasons observed at Gadanki (present study) compared with other global sites based on Andreae [2]. The black line indicates the best fit and the upper error bars extend to the 75th percentile and lower bars to the 25th percentile

measurement cycle of 5 min, was calculated on a size grid between 10 nm and 400 nm (39 equidistant bins). As can be seen from Fig. 6a, during the BoB air mass more than 85% of the time the geometric mean diameter was between 60 to 160 nm and ~ 7% of the geometric mean diameter at less than 50 nm. The 80 nm diameter exhibited a maximum occurrence of around 23%. On the other hand, the frequency distribution of geometric mean diameter for AS air mass showed a different picture with the geometric mean diameter being less than 50 nm for ~ 45% of the time and in the range of 60–160 nm for ~ 50% of the time.

To investigate further if any of the meteorological parameters exhibited a strong relation with particle size, we derived a correlation between geometric mean diameter and relative humidity (Fig. S5). A relatively strong correlation coefficient of $R^2 = 0.87$ between geometric mean diameter and relative humidity was found during the AS air mass, whereas the correlation for the BoB air mass was observed to be relatively weak ($R^2 = 0.10$). The increase in relative humidity might have caused the hygroscopic growth of the pre-existing aerosol particles [19]. Due to the distinct origin of air masses (AS vs. BoB), the hygroscopicity of the aerosol particles may vary owing to ageing and continental influence. In view of the low variability of the aerosol numbers, the resulting variance in droplet number concentration is a function of updraft velocity alone and independent of changes in chemical composition, for example, as reported by Bougiatioti et al. [7] for a remote background site in Eastern Mediterranean. The variance in cloud droplet number concentration was largely independent of κ. However, further investigations using a hygroscopic tandem differential mobility analyser (HTDMA), which was not available for the present study, may be required to shed some detailed insight on this aspect. The exact physical and chemical relations behind this strong correlation could not be explained with the available data and information.

3.3 Cloud condensation nuclei (CCN) number estimation

In the present study, the $CCN_{0.4}$ concentrations were estimated as described in Sect. 2.3. The relation between $CCN_{0.4}$ and the total particle number concentration averaged over May to July 2012 at Gadanki is individually depicted in Fig. 7 and is compared with other global sites as compiled by Andreae [2]. The CN and $CCN_{0.4}$ number concentration at Gadanki during May was in the same range as concentrations observed at other polluted locations across the globe. We hypothesize that this partly results from the low critical dry diameter (66 nm) as compared to other similar sites, which was derived as cut-off diameter with the assumption of $\kappa = 0.3$ at a supersaturation level of 0.4%, as the shape of the particle number

Table 2 CN and CCN number concentrations in May and June–July showing the substantial decrease in the concentration during the monsoon season

Season	$N_{Tot_}$CCN (cm^{-3})	$N_{Tot_}$CN (cm^{-3})	CCN/CN
May (pre-monsoon)	3540	5870	0.60
June–July (monsoon)	1541	4075	0.38

size distribution strongly affects the value of $CCN_{0.4}$. For example, during May, a large proportion of particles were in the higher Aitken mode range (geometric mean diameter = 88 ± 1.4), thus making more particles available for CCN activation, as they are larger than the critical diameter. The calculated $CCN_{0.4}$ concentrations are mostly sensitive to variations in N_{Acc} and vary accordingly between the May and June–July.

The CN number concentration June–July was reduced by 31% compared to May, and a substantial difference (57%) in the $CCN_{0.4}$ was observed (as seen in Table 2) as evident from the $CCN_{0.4}$/CN ratio. This can be partly explained based on the difference in the geometric mean diameter and shape of the particle number size distribution during May and June–July. The geometric mean diameters during June and July (50 nm, and 20 and 60 nm, respectively) were smaller than the critical dry diameter (66 nm) as compared to the month of May, implying more particles were in the lower Aitken mode (and nucleation mode range for July) range. These particles were not able to activate as CCN, because they were smaller than the critical dry diameter, and relatively fewer particles contributed to the CCN concentration. Note, however, that detailed size-resolved CCN measurements supplemented by chemical composition could provide a more detailed picture about the CCN properties of atmospheric aerosols at this site. Nevertheless, the variation of $CCN_{0.4}$ for May and June–July indicated the strong influence of the shape of the particle number size distribution and geometric mean diameter. This conclusion is consistent with previous studies reporting that the size of the aerosol particles is the most important factor for activation as CCN at a given supersaturation [1, 11, 16, 17, 27, 36, 47, 48]).

3.4 Cloud parcel modelling

To investigate the possible implications of aerosol particle number size distribution and updraft velocity on the CCN activation and subsequent droplet formation at cloud base during the two distinct seasons, cloud parcel model runs were performed separately for May and June–July. The simulations were performed using the input parameters given in Table S2.

Figure 8 shows the cloud droplet number concentration, N_{CD}, the maximum water vapour supersaturation reached in the ascending air mass (S_{max}), and the corresponding activated fraction of the initial aerosol particle concentration, for May and June–July, simulated by the cloud parcel model as described in Sect. 2.3. The N_{CD} isolines shown in Fig. 8a for the month of May are plotted covering the full range of updraft velocity and particle number concentration as input to the model so as to allow a generic comparison with the most polluted sites, where the particle number concentration is reaching as high as 15×10^3 cm^{-3}. Based on the average observed aerosol particle concentration range (3×10^3–4.5×10^3 cm^{-3}) and updraft velocity range (4–6 m s^{-1}; [44, 61] during May, the regime in Gadanki shifted from the aerosol-limited regime to the transitional regime, where a relatively high ratio between updraft velocity and particle number concentration (lower left corner of Fig. 8a) is observed (0.83×10^{-3} ms^{-1} cm^3). Even though the site falls mostly into the transitional regime, it is close to the aerosol-limited regime. It is associated with a high activated fraction of aerosol particles ($N_{CD}/N_{CN} > \approx 70\%$; Fig. 8e), and the maximum values of water vapour supersaturation (S_{max}) were between 0.20 and 0.30% as shown in Fig. 8c. These values of activated fraction and S_{max} were lower than in the pristine Amazonian region ($N_{CD}/N_{CN} = 80\%$ and $S_{max} = 1.5\%$) and higher than in the highly polluted megacity of Beijing ($N_{CD}/N_{CN} = 20\%$ and $S_{max} = 0.1\%$) [16, 17]. In the aerosol-limited regime, N_{CD} is directly proportional to the initial aerosol particle number concentration [9, 45].

During June–July, the observed initial particle number concentration was similar to May, but the updraft velocities were a little lower (1–2 m s^{-1}; [44, 61]. Thus, the CCN activation and N_{CD} formation were in the transitional regime (Fig. 8b) with $\omega/N_{CN} = 0.30 \times 10^{-3}$ ms^{-1} cm^3. The transitional regime during June–July was characterized by an activated fraction (N_{CD}/N_{CN}) greater than 45%, with a maximum value of ~ 70%, compared to 90% during May. Interestingly, the water vapour supersaturation (S_{max}) was between 0.1 and 0.15%, with a maximum value of 0.80%, in contrast to the maximum value of 0.60% during the month of May. The shape of the particle number size distribution observed during the two seasons could partially explain this. The geometric mean diameter ($D_g = 89$ nm) during the month of May was higher than during June–July ($D_{g1} = 25$ nm and $D_{g2} = 55$ nm). This in turns means that during May, the geometric mean diameter was larger than the critical dry diameter (66 nm) required for the CCN activation at the given supersaturation (0.4%) and hygroscopicity parameter ($\kappa = 0.3$), but during June–July it was lower. Hence, during June–July there were a larger number of smaller particles, which were not able to activate as CCN, whereas during May, particles in the larger size range

dominated. This can also explain the lower S_{max} during June–July, as a higher number of smaller particles caused depleted water vapour supersaturation, and they were not able to grow large enough to be activated as cloud droplets. Broadly, the cloud formation regime over Gadanki falls between clean Amazon rainforest air (aerosol-limited) and highly polluted Beijing megacity air (updraft-limited) and is strongly dependent on the particle number concentration and size distribution [16, 17]. Global modelling studies suggest that the aerosol-limited regimes may be more similar to clean marine clouds, whereas the updraft-limited regimes may be more characteristic of polluted continental clouds [12, 46, 51]. The cloud droplet formation is initiated by nucleation at cloud base and is the major factor that controls cloud droplet number concentration [9]. Thus, the effect of aerosol on cloud is regime dependent and based on the meteorological conditions, cloud types, and aerosol properties [59].

4 Summary and conclusions

We presented 3 months of continuous measurements of particle number size distribution from a semi-rural site, Gadanki, in southern tropical India during the transition from May to June–July. During May, the total particle number concentration was higher by 69% and the shape of the size distribution was monomodal with a narrow peak. The geometric mean diameter was larger than in June–July, which has implications on CCN activation and cloud droplet formation. The relative contribution from different modes of the number size distribution exhibited a strong variability during the two distinct seasons. The relative contribution from Aitken mode particles remained constant during the entire measurement period. The difference in the particle number size distributions pointed towards the possibility of different particle sources during May and June–July. When the air masses originated over the Bay of Bengal, the particle number size distribution was narrower ($D_g = 83$ nm) and the number concentration was 25% higher than during air masses from the Arabian Sea, which had a bimodal particle number size distribution ($N_{tot} = 4.6 \times 10^3$ cm^{-3}; $D_{g1} = 30$ nm, and $D_{g2} = 70$ nm) indicating an effect of different air mass origin on particle number size distribution. Thus, the particle number concentration at the site was not significantly affected by local emissions and hence can be regarded as semi-rural. The diurnal variation in the two distinct air masses also exhibited a pronounced diurnal variation, which was consistent with the meteorology. Interestingly, an increase in geometric mean diameter in the AS air mass was strongly correlated with relative humidity.

Based on cloud parcel model simulations, we found marginal differences in the ω/N_{CN} ratios and cloud formation regimes between May and June–July. The cloud formation during May was classified between the aerosol-limited regime and the transitional regime, while during June–July, we found cloud formation to be in the transitional regime. These regimes were classified depending on the ratio between updraft velocity and particle number concentration (ω/N_{CN}) as presented by Reutter et al. [45]. In general, the model results suggested that the variability of the initial cloud droplet number concentration at cloud base was dominated by the updraft velocity and aerosol particle number concentration in the accumulation mode. These conclusions are consistent with previous studies reporting a greater importance of the shape of the particle number size distribution over their composition for the activation of aerosol particles as CCN and cloud droplets. However, for better elucidation of the role of aerosols on cloud and precipitation formation over this region, 3D model simulations for the specific seasonal conditions at Gadanki as reported by Chang et al. [9] should be considered.

In conclusion, the particle number size distribution measurements carried out at Gadanki, a semi-rural site in tropical southern India, revealed very different characteristics in terms of the shape of the particle number size distribution with relatively small changes in the number concentration during the two distinct seasons. This indicates the dominance of distinct sources during the different seasons in this region. Note that the data presented in this study are limited to this particular environment and time of the year and cannot be extrapolated to larger spatio-temporal scales. We recommend long-term particle number size distribution measurements over similar and other regions in India to help in understanding the role of various sources in aerosol formation and their role in the climate over this region.

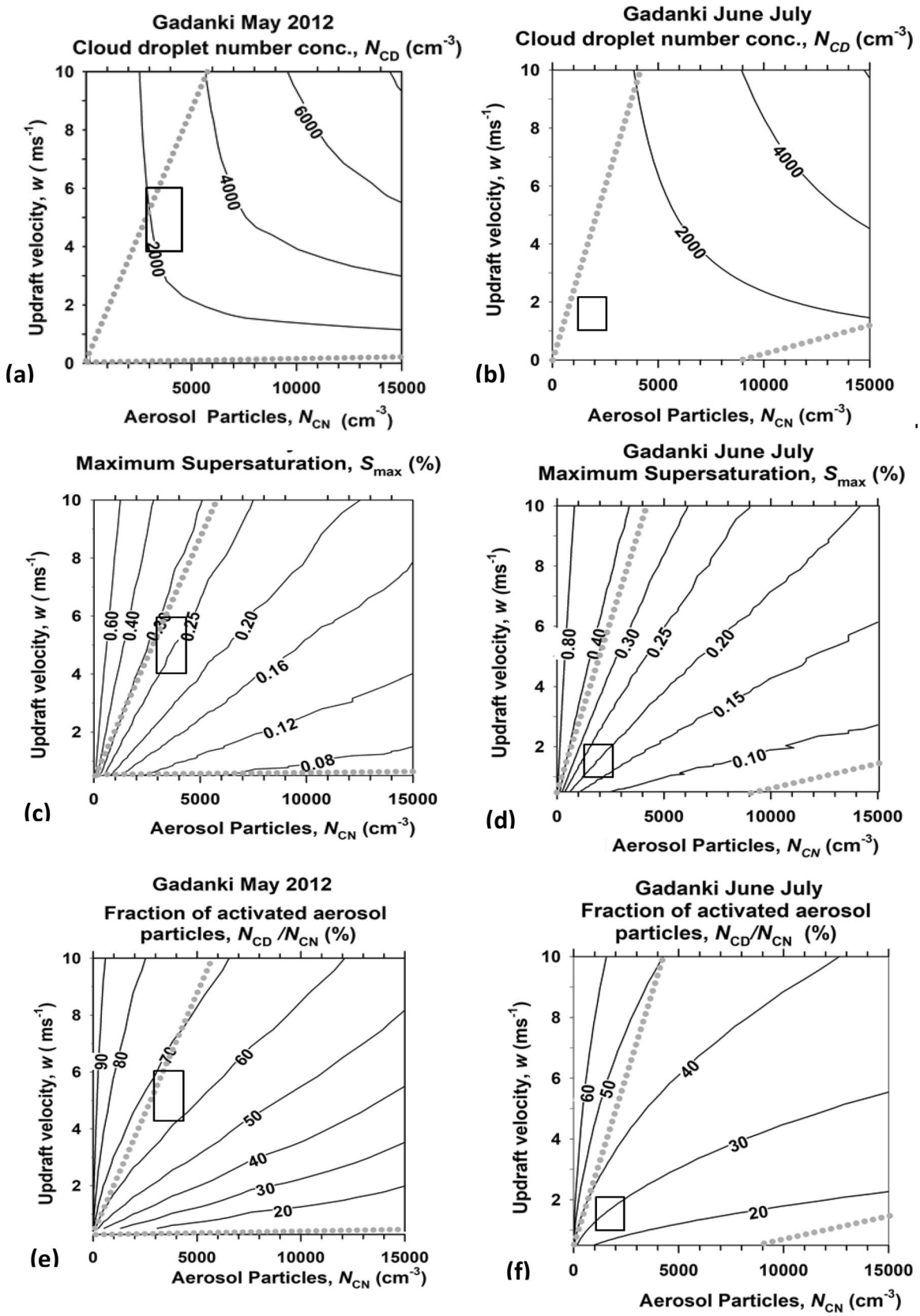
Gadanki May 2012
Cloud droplet number conc., N_{CD} (cm^{-3})
Updraft velocity, w (ms^{-1})
Aerosol Particles, N_{CN} (cm^{-3})
6000
4000
2000
(a)
Gadanki June July
Cloud droplet number conc., N_{CD} (cm^{-3})
4000
2000
(b)
Maximum Supersaturation, S_{max} (%)
0.60
0.40
0.30
0.25
0.20
0.16
0.12
0.08
(c)
Gadanki June July
Maximum Supersaturation, S_{max} (%)
0.80
0.40
0.30
0.25
0.20
0.15
0.10
(d)
Gadanki May 2012
Fraction of activated aerosol particles, N_{CD}/N_{CN} (%)
90
80
70
60
50
40
30
20
(e)
Gadanki June July
Fraction of activated aerosol particles, N_{CD}/N_{CN} (%)
60
50
40
30
20
(f)

◂**Fig. 8** Location of the Gadanki site (shown as open square box) in the regime space defined by aerosol particle concentration, updraft velocity, and cloud droplet number concentration. The contours represent cloud droplet number concentration (**a**, **b**), maximum supersaturation (**c**, **d**) and fraction of activated particles (**e**, **f**) for the pre-monsoon (May) and monsoon (June–July) periods. The dotted lines in the figure indicate the approximate border line between the regimes. The region above the upper dotted line represents the aerosol-limited regime, below the lower dotted line the updraft-limited regime, and in between the two lines the transitional regime

Acknowledgements SSG would like to acknowledge the financial support from DST-Max Planck Partner Group at IIT Madras, Department of Science and Technology, Govt. of India, and Ministry of Earth Sciences, Govt. of India, for carrying out this campaign. The authors are grateful to Ulrich Pöschl, M. O. Andreae, Hang Su, Diana Rose, Christopher Pöhlker, and Mira Pöhlker for providing the modified cloud parcel model and their suggestions during entire course of this study and valuable inputs for manuscript writing. Authors acknowledge the support from Mr. Rohit for his support during the field campaign. SS gratefully acknowledges the fellowship from MHRD, Govt. of India. Authors are thankful to two anonymous Referees for their valuable suggestions and insights during the review process.

Compliance with ethical standards

Conflict of interest On behalf of all authors, the corresponding author states that there is no conflict of interest.

References

1. Andreae MO, Rosenfeld D (2008) Aerosol-cloud-precipitation interactions. Part 1. The nature and sources of cloud-active aerosols. Earth Sci Rev 89:13–41
2. Andreae MO (2009) Correlation between cloud condensation nuclei concentration and aerosol optical thickness in remote and polluted regions. Atmos Chem Phys 9:543–556
3. Andreae MO, Hegg D, Baltensperger U (2009) Sources and nature of atmospheric aerosols. In: Levin Z, Cotton W (eds) Aerosol pollution impact on precipitation: a scientific review. Springer, Berlin, pp 45–89
4. Asmi A, Wiedensohler A, Laj P, Fjaeraa AM, Sellegri K, Birmili W, Kulmala M (2011) Number size distributions and seasonality of submicron particles in Europe 2008–2009. Atmos Chem Phys 11:5505–5538
5. Belosi F, Contini D, Donateo A, Santachiara G, Prodi F (2012) Aerosol size distribution at Nansen Ice Sheet Antarctica. Atmos Res 107:42–50
6. Biagio CD, Doppler L, Gaimoz C, Grand N, Ancellet G, Raut J, Beekmann M, Borbon A, Wetterdienst D, Lindenberg MO (2015) Continental pollution in the western Mediterranean basin: vertical profiles of aerosol and trace gases measured over the sea during TRAQA 2012 and SAFMED 2013. Atmos Chem Phys 15:9611–9630
7. Bougiatioti A, Bezantakos S, Stavroulas I, Kalivitis N, Kokkalis P, Biskos G, Mihalopoulos N, Papayannis A, Nenes A (2016) Biomass-burning impact on CCN number, hygroscopicity and cloud formation during summertime in the eastern Mediterranean. Atmos Chem Phys 16:7389–7409
8. Braga RC, Rosenfeld D, Weigel R, Jurkat T, Andreae MO, Wendisch M, Pöschl U, Voigt C, Mahnke C, Borrmann S, Albrecht RI, Molleker S, Vila DA, Machado LAT, Grulich L (2017) Aerosol concentrations determine the height of warm rain and ice initiation in convective clouds over the Amazon basin. Atmos Chem Phys Discuss 17:14433–14456
9. Chang D, Cheng Y, Reutter P, Trentmann J, Burrows SM, Spichtinger P, Nordmann S, Andreae MO, Pöschl U, Su H (2014) Comprehensive mapping and characteristic regimes of aerosol effects on the formation and evolution of pyro-convective clouds. Atmos Chem Phys 15:10325–10348
10. Cheng CT, Wang WC, Chen JP (2010) Simulation of the effects of increasing cloud condensation nuclei on mixed-phase clouds and precipitation of a front system. Atmos Res 96:461–476
11. Dusek U, Frank GP, Hildebrandt L, Curtius J, Schneider J, Walter S, Andreae MO (2006) Size matters more than chemistry aerosol particles. Science 312(June):1375–1378
12. Fan JW, Leung LR, Rosenfeld D, Chen Q, Li ZQ, Zhang JQ, Yan HR (2013) Microphysical effects determine macrophysical response for aerosol impacts on deep convective clouds. Proc Natl Acad Sci USA 110:E4581–E4590
13. Freutel F, Schneider J, Drewnick F, Von Der Weiden-Reinmüller SL, Crippa M, Prévôt SH, Borrmann S (2013) Aerosol particle measurements at three stationary sites in the megacity of Paris during summer 2009: meteorology and air mass origin dominate aerosol particle composition and size distribution. Atmos Chem Phys 13:933–959
14. Gadhavi HS, Renuka K, Ravi Kiran V, Jayaraman A, Stohl A, Klimont Z, Beig G (2015) Evaluation of black carbon emission inventories using a Lagrangian dispersion model: a case study over southern India. Atmos Chem Phys 15:1447–1461
15. Ganguly D, Jayaraman A, Gadhavi H, Rajesh TA (2005) Features in wavelength dependence of aerosol absorption observed over central India. Geophys Res Lett 32:1–4
16. Gunthe SS, King SM, Rose D, Chen Q, Roldin P, Farmer DK, Jimenez JL, Artaxo P, Andreae MO, Martin ST, Pöschl U (2009) Cloud condensation nuclei in pristine tropical rainforest air of Amazonia: size-resolved measurements and modeling of atmospheric aerosol composition and CCN activity. Atmos Chem Phys Discuss 9:3811–3870
17. Gunthe SS, Rose D, Su H, Garland RM, Achtert P, Nowak A, Wiedensohler A, Kuwata M (2011) Cloud condensation nuclei (CCN) from fresh and aged air pollution in the megacity region of Beijing. Atmos Chem Phys 11:11023–11039
18. Guo H, Wang DW, Cheung K, Ling ZH, Chan CK, Yao XH (2012) Observation of aerosol size distribution and new particle formation at a mountain site in subtropical Hong Kong. Atmos Chem Phys 12:9923–9939
19. Hamed A, Korhonen H, Sihto SL, Joutsensaari J, Jrvinen H, Petäjä T, Laaksonen A (2011) The role of relative humidity in continental new particle formation. J Geophys Res Atmos 116:1–12
20. Hazra A, Goswami BN, Chen J-P (2013) Role of interactions between aerosol radiative effect, dynamics, and cloud microphysics on transitions of monsoon intraseasonal oscillations. J Atmos Sci 70:2073–2087
21. Heintzenberg J, Covert D, Van Dingenen R (2000) Size distribution and chemical composition of marine aerosols: a compilation and review. Tellus B 52:1104–1122
22. Hyvärinen AP, Raatikainen T, Komppula M, Mielonen T, Sundström AM, Brus D, Lihavainen H (2011) Effect of the summer monsoon on aerosols at two measurement stations in Northern India-Part 2: physical and optical properties. Atmos Chem Phys 11:8283–8294
23. Jayaraman A, Gadhavi H, Ganguly D, Misra A, Ramachandran S, Rajesh TA (2006) Spatial variations in aerosol characteristics

and regional radiative forcing over India: measurements and modeling of 2004 road campaign experiment. Atmos Environ 40:6504–6515
24. Kanawade VP, Benson DR, Lee SH (2012) Statistical analysis of 4-year observations of aerosol sizes in a semi-rural continental environment. Atmos Environ 59:30–38
25. Kanawade VP, Shika S, Pöhlker C, Rose D, Suman MNS, Gadhavi H, Kumar A, Nagendra SMS, Ravikrishna R, Yu H, Sahu LK, Jayaraman A, Andreae MO, Pöschl U, Gunthe SS (2014) Infrequent occurrence of new particle formation at a semi-rural location, Gadanki, in tropical Southern India. Atmos Environ 94:264–273
26. Kanawade VP, Tripathi SN, Bhattu D, Shamjad PM (2014) Submicron particle number size distributions characteristics at an urban location, Kanpur, in the Indo-Gangetic Plain. Atmos Res 147–148:121–132
27. Kim N, Park M, Yum SS, Park JS, Song IH, Shin HJ, Ahn JY, Kwak KH, Kim H, Bae GN, Lee G (2017) Hygroscopic properties of urban aerosols and their cloud condensation nuclei activities measured in Seoul during the MAPS-Seoul campaign. Atmos Environ 153:217–232
28. Kompalli SK, Babu SS, Moorthy KK, Gogoi MM, Vijaykumar S, Chaubey JP (2014) The formation and growth of ultrafine particles in two contrasting environments: a case study. Ann Geophys 32:817–830
29. Komppula M, Lihavainen H, Hyvärinen AP, Kerminen VM, Panwar TS, Sharma VP, Viisanen Y (2009) Physical properties of aerosol particles at a Himalayan background site in India. J Geophys Res 114:D12202
30. Kopanakis I, Chatoutsidou SE, Torseth K, Glytsos T, Lazaridis M (2013) Particle number size distribution in the eastern Mediterranean: formation and growth rates of ultrafine airborne atmospheric particles. Atmos Environ 77:790–802
31. Kulmala M, Kontkanen J, Junninen H, Lehtipalo K, Manninen HE, Nieminen T, Petäjä T, Sipilä M, Schobesberger S, Rantala P, Franchin A, Jokinen T, Järvinen E, Äijälä M, Kangasluoma J, Hakala J, Aalto PP, Paasonen P, Mikkilä J, Vanhanen J, Aalto J, Hakola H, Makkonen U, Ruuskanen T, Mauldin RL, Duplissy J, Vehkamäki J, Bäck J, Kortelainen A, Riipinen I, Kurtén T, Johnston MV, Smith JN, Ehn M, Mentel TF, Lehtinen KEJ, Laaksonen A, Kerminen V, Worsnop DR (2013) Direct observations of atmospheric aerosol nucleation. Sciences 339:943–946
32. Kulmala M, Petäjä T, Nieminen T, Sipilä M, Manninen HE, Lehtipalo K, Dal Maso M, Aalto PP, Junninen H, Paasonen P, Riipinen I, Lehtinen KEJ, Laaksonen A, Kerminen V (2012) Measurement of the nucleation of atmospheric aerosol particles. Nat Protoc 7:1651–1667
33. Leng C, Cheng T, Chen J, Zhang R, Tao J, Huang G, Zha S, Zhang M, Fang W, Li X, Li L (2013) Measurements of surface cloud condensation nuclei and aerosol activity in downtown Shanghai. Atmos Environ 69:354–361
34. Lin P, Hu M, Wu Z, Niu Y, Zhu T (2007) Marine aerosol size distributions in the springtime over China adjacent seas. Atmos Environ 41:6784–6796
35. Mauritsen T, Sedlar J, Tjernstrom M, Leck C, Martin M, Shupe M, Sjogren S, Sierau B, Persson POG, Brooks IM, Swietlicki E (2011) An arctic CCN-limited cloud-aerosol regime: atmos. Chem Phys 11:165–173
36. Miao Q, Zhang Z, Li Y, Qin X, Xu B, Yuan Y, Gao Z (2015) Measurement of cloud condensation nuclei (CCN) and CCN closure at Mt. Huang based on hygroscopic growth factors and aerosol number-size distribution. Atmos Environ 113:127–134
37. Mönkkönen P, Koponen IK, Lehtinen KEJ, Hämeri K, Uma R, Kulmala M (2005) Measurements in a highly polluted Asian mega city: observations of aerosol number size distribution, modal parameters and nucleation events. Atmos Chem Phys 5:57–66
38. Murugavel P, Chate DM (2009) Generation and growth of aerosols over Pune, India. Atmos Environ 43(4):820–828
39. Nishita C, Osada K, Kido M, Matsunaga K, Iwasaka Y (2008) Nucleation mode particles in upslope valley winds at Mount Norikura, Japan: implications for the vertical extent of new particle formation events in the lower troposphere. J Geophys Res Atmos 113:1–10
40. Patil N, Dave P, Venkataraman C (2017) Contrasting influences of aerosols on cloud properties during deficient and abundant monsoon years. Sci Rep. https://doi.org/10.1038/srep44996
41. Petters MD, Kreidenweis SM (2007) A single parameter representation of hygroscopic growth and cloud\ncondensation nucleus activity. Atmos Chem Phys 7:1961–1971
42. Pringle KJ, Tost H, Pozzer A, Pöschl U, Lelieveld J (2010) Global distribution of the effective aerosol hygroscopicity parameter for CCN activation. Atmos Chem Phys 10:5241–5255
43. Ramanathan V, Chung C, Kim D, Bettge T, Buja L, Kiehl JT, Washington WM, Fu Q, Sikka DR, Wild M (2005) Atmospheric brown clouds: impacts on South Asian climate and hydrological cycle. PNAS 102(15):5326–5333
44. Rao TN, Uma KN, Satyanarayana TM, Rao DN (2009) Differences in draft core statistics from the wet to dry spell over Gadanki, India (13.5° N, 79.2° E). Mon Weather Rev 137:4293–4306
45. Reutter P, Trentmann J, Su H, Simmel M, Rose D, Wernli H, Pöschl U (2009) Aerosol- and updraft-limited regimes of cloud droplet formation: influence of particle number, size and hygroscopicity on the activation of cloud condensation nuclei (CCN). Atmos Chem Phys Discuss 9:8635–8665
46. Roberts GC, Andreae MO, Zhou J, Artaxo P (2001) Cloud condensation nuclei in the Amazon Basin: "Marine" conditions over a continent? Geophys. Res. Lett. 28:2807–2810
47. Rose D, Gunthe SS, Mikhailov E, Frank GP, Dusek U, Andreae MO, Pöschl U (2008) Calibration and measurement uncertainties of a continuous-flow cloud condensation nuclei counter (DMT-CCNC): CCN activation of ammonium sulfate sodium chloride aerosol particles in theory and experiment. Atmos Chem Phys 8:1153–1179
48. Rose D, Nowak A, Achtert P, Wiedensohler A, Hu M, Shao M, Zhang Y, Andreae MO, Pöschl U (2010) Cloud condensation nuclei in polluted air and biomass burning smoke near the mega-city Guangzhou, China—Part 1: size-resolved measurements and implications for the modeling of aerosol particle hygroscopicity and CCN activity. Atmos Chem Phys 10:3365–3383
49. Rosenfeld D, Lohmann U, Raga GB, Dowd CDO, Kulmala M, Fuzzi S, Reissell A, Andreae MO (2008) Flood or drought: how do aerosols affect precipitation? Science 321:1309–1313
50. Sarangi C, Kanawade V, Tripathi SN, Thomas A, Ganguly D (2018) Aerosol-induced intensification of cooling effect of clouds during Indian Summer Monsoon. Nat Commun 9:3754
51. Seifert A, Kohler C, Beheng KD (2012) Aerosol-cloud precipitation effects over Germany as simulated by a convective scale numerical weather prediction model. Atmos Chem Phys 12:709–725
52. Seinfeld JH, Pandis SN (2006) Atmospheric chemistry and physics: from air pollution to climate change, 2nd edn. Wiley, New York
53. Shen XJ, Sun JY, Zhang YM, Wehner B, Nowak A, Tuch T, Zhang XC, Wang TT, Zhou HG, Zhang XL, Dong F, Birmili W, Wiedensohler A (2011) First long-term study of particle number size distributions and new particle formation events of regional aerosol in the North China Plain. Atmos Chem Phys 11:1565–1580
54. Shrestha P, Barros AP, Khlystov A (2010) Chemical composition and aerosol size distribution of the middle mountain range in the Nepal Himalayas during the 2009 pre-monsoon season. Atmos Chem Phys 10:11605–11621

55. Simmel M, Trautmann T, Tetzlaff G (2002) Numerical solution of the stochastic collection equation—comparisons of the Linear Discrete Method with other methods. Atmos Res 61:135–148
56. Simmel M, Wurzler S (2006) Condensation and activation in sectional cloud microphysical models. Atmos Res 80:218–236
57. Sorribas M, De La Morena BA, Wehner B, López JF, Prats N, Mogo S, Cachorro VE (2011) On the sub-micron aerosol size distribution in a coastal-rural site at El Arenosillo Station (SW-Spain). Atmos Chem Phys 11:11185–11206
58. Stein AF, Draxler RR, Rolph GD, Stunder BJB, Cohen MD, Ngan F (2015) NOAA's HYSPLIT atmospheric transport and dispersion modeling system. Bull Am Meteorol Soc 96:2059–2077
59. Tao WK, Chen JP, Li ZQ, Wang C, Zhang CD (2014) Impact of aerosols on convective clouds and precipitation. Rev Geophys 50:2001
60. Tunved P, Ström J, Hansson HC (2004) An investigation of processes controlling the evolution of the boundary layer aerosol size distribution properties at the Swedish background station Aspvreten. Atmos Chem Phys Discuss 4:4507–4543
61. Uma KN, Kumar KK, Shankar Das S, Rao TN, Satyanarayana TM (2012) On the vertical distribution of mean vertical velocities in the convective regions during the wet and dry spells of the monsoon over Gadanki. Mon Weather Rev 140:398–410
62. Wang ZB, Hu M, Sun JY, Wu ZJ, Yue DL, Shen XJ, Wiedensohler A (2013) Characteristics of regional new particle formation in urban and regional background environments in the North China Plain. Atmos Chem Phys 13:12495–12506